Quantum mold casting for topological insulating and edge states

X. M. Yang and Z. Song*
School of Physics, Nankai University, Tianjin 300071, China

(Received 3 January 2021; accepted 15 March 2021; published 23 March 2021)

We study the possibility of transferring fermions from a trivial system as a particle source to an empty system but in the topological phase as a mold for casting a stable topological insulator dynamically. We show that this can be realized by a non-Hermitian unidirectional hopping, which connects a central system at topological phase and a trivial flat-band system with a periodic driving chemical potential, which scans over the valence band of the central system. The near exceptional point dynamics allows a unidirectional dynamical process: the time evolution from an initial state with a fully filled source system to approximately a stable topological insulating state. The result is demonstrated numerically by a source-assistant Qi-Wu-Zhang model and Su-Schrieffer-Heeger chain in the presence of random perturbation. Our finding reveals a classical analogy of quench dynamics in quantum matter and provides a way for topological quantum state engineering.

DOI: 10.1103/PhysRevB.103.094307

I. INTRODUCTION

Preparing a topologically nontrivial state is of great interest for the task of quantum information processing. In general, a natural way to prepare a topological insulating state is cooling a system down to its ground state by suppressing the thermal fluctuations. Another intuitive way for the preparation of a topological insulating state is to follow a mechanical way by filling the topological energy band with fermions dynamically. However, it is tough to move fermions one by one from a particle source to an empty system since fermions obey the Schrodinger equation rather than Newton's laws. Recently, a dynamical way of realizing the topological phases by applying time-periodic global driving on a topologically trivial initial state was proposed. It has been shown that these periodic perturbations lead to the realization of new topological phases of matter which have no equilibrium counterparts [1–6], including topological insulators [7,8] and edge states [9,10]. It opens up a way to realize a topological phase dynamically. In the studies above, both the effective Hamiltonian dictating the nonequilibrium dynamics of the system and the initial static Hamiltonian are Hermitian. Nevertheless, a non-Hermitian Hamiltonian is no longer forbidden both in theory and experiment since the discovery that a certain class of non-Hermitian Hamiltonians could exhibit entirely real spectra [11,12]. The origin of the reality of the spectrum of a non-Hermitian Hamiltonian is the pseudo-Hermiticity of the Hamiltonian operator [13]. It motivates a non-Hermitian extension of the dynamical preparation of a topologically nontrivial state. In addition, the peculiar features of a non-Hermitian system manifest not only in statics but also dynamics. Non-Hermitian systems exhibit many peculiar dynamic behaviors that never occur in Hermitian systems. One of the remarkable features is the dynamics at the exceptional point (EP) [14–16] or spectral singularity [17–21], where the system has a coalescence state. Exclusively, EP dynamics recently emerged as a transformative tool for dynamically evolving quantum systems into a quantum phase with desirable properties [22–24]. It is expected that the introduction of non-Hermitian elements benefits the scheme for quantum state engineering.

In this work, we focus on the EP-related dynamic behavior for the many-body system. From the perspective of non-Hermitian quantum mechanics, it is also a challenge to deal with many-particle dynamics. As an application, we study the possibility of transferring fermions from a trivial system as a particle source to an empty system but in the topological phase as a mold for casting a stable topological insulator dynamically. We show that this can be realized by a non-Hermitian connection between a central system in the topological phase and a flat-band system with a periodic driving chemical potential. After a sufficiently long time, the near exceptional point dynamics allows the time evolution from an initial state with a fully filled source system to approximately a stable topological insulating state. Schematics for the system and process of quantum mold casting are presented in Fig. 1. We demonstrate the scheme by numerical simulations for a source-assistant Qi-Wu-Zhang (QWZ) model and Su-Schrieffer-Heeger (SSH) chain in the presence of random perturbation. The result reveals a classical analogy of quench dynamics in quantum matter and provides a method for topological quantum state engineering. It also shows that a unidirectional tunneling supports an exclusive feature that never occurs in a Hermitian system, which can be utilized for quantum state engineering. Our findings pave the way for establishing EP dynamics based techniques as a powerful and versatile tool for topological state engineering.

This paper is organized as follows. In Sec. II, we describe the model Hamiltonian and give the conditions for the existence of the coalescing state. In Sec. III, based on the solutions, we present the characteristics of the EP dynamics in a source-assistant QWZ model and the details of

*songtc@nankai.edu.cn

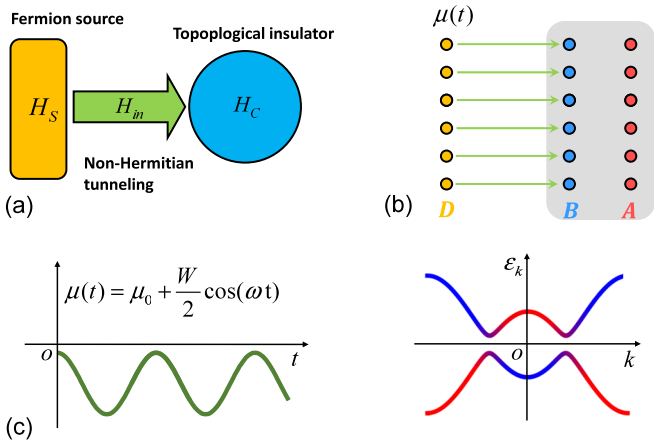

FIG. 1. Schematics for the system and process of quantum mold casting. (a) The system consists of two parts, the central system H_c and the source system H_s. The target state is the ground state of H_c, which can be topologically nontrivial or not. H_s is a topologically trivial system, providing the supply of fermions. Both H_c and H_s are Hermitian, while H_{in} is non-Hermitian, representing the connection between H_c and H_s and taking on the job of transporting fermions unidirectionally from H_s to H_c. (b) A tight-binding model for the scheme, which contains three sets, A, B, and D. Lattices A and B (red and blue solid circles) embedded in the shadow area are topological insulators, while lattice D (yellow solid circles) is a flat-band (hopping-free) system but with an oscillating chemical potential. Green arrows represent unidirectional hopping from the D to B lattice. The aim of this work is to realize the following process via time evolution. Initially, the D lattice is fully filled, while A and B are empty. The final state is expected to be a half-filled ground state of H_c. (c) The underlying mechanism of the dynamic process. At instant $t_{\mathbf{k}}$, the chemical potential and energy levels of H_c are resonant, leading to exceptional points. The corresponding (EP) dynamics allows a complete transfer of fermions between the degenerate energy levels. In the long-time limit, such dynamics occurs at each $\mathbf{k}$ sector again and again. The band color of H_c illustrates the band inversion, indicating that the energy band can be a topological insulating band [25]. It is expected that the lower band of H_c can be completely filled.

the dynamical formation of a topological insulating state. In Sec. IV, we propose a dynamical way to cast edge states in a source-assistant Rice-Mele (RM) model. Finally, we give a summary and discussion in Sec. V.

II. MODEL AND COALESCING STATE

We consider a non-Hermitian time-dependent Hamiltonian

$$H = H_c + H_s + H_{in}, \tag{1}$$

with

$$H_c = \sum_{i,j=1}^{N} \left(T_{ij} a_i^\dagger b_j + A_{ij} a_i^\dagger a_j + B_{ij} b_i^\dagger b_j + \text{H.c.}\right) \tag{2}$$

and

$$H_s = \mu(t) \sum_{j=1}^{N} d_j^\dagger d_j, H_{in} = \gamma \sum_{j=1}^{N} b_j^\dagger d_j, \tag{3}$$

where a_j, b_j, and d_j are fermion operators and $\mu(t) = \mu_0 + \frac{W}{2}\cos(\omega t)$ is the periodic driving chemical potential, with parameters $\{T_{ij}, A_{ij}, B_{ij}\}$ depending on H_c (μ_0 is an average of the negative energy levels and W is the bandwidth of H_c). Here, both H_c and H_s are Hermitian, describing the central system and source system, respectively. Notably, H_{in} is a non-Hermitian term, representing the connection between the two systems, H_c and H_s.

For a central system with the periodic boundary condition, after performing Fourier transformation, we have $H = \sum_{\mathbf{k}} H_{\mathbf{k}}$, where the sub-Hamiltonian $H_{\mathbf{k}}$ in each invariant subspace can be expressed as

$$H_{\mathbf{k}} = \begin{pmatrix} a_{\mathbf{k}}^\dagger & b_{\mathbf{k}}^\dagger & d_{\mathbf{k}}^\dagger \end{pmatrix} h_{\mathbf{k}} \begin{pmatrix} a_{\mathbf{k}} \\ b_{\mathbf{k}} \\ d_{\mathbf{k}} \end{pmatrix}, \tag{4}$$

where

$$\begin{pmatrix} a_{\mathbf{k}}^\dagger & b_{\mathbf{k}}^\dagger & d_{\mathbf{k}}^\dagger \end{pmatrix} = \sum_{\mathbf{r}} \frac{e^{i\mathbf{k}\cdot\mathbf{r}}}{\sqrt{N}} \begin{pmatrix} a_{\mathbf{r}}^\dagger & b_{\mathbf{r}}^\dagger & d_{\mathbf{r}}^\dagger \end{pmatrix}. \tag{5}$$

In general, the Bloch matrix $h_{\mathbf{k}}$ has the form

$$h_{\mathbf{k}} = \begin{pmatrix} B_z(\mathbf{k}) & B_x(\mathbf{k}) - iB_y(\mathbf{k}) & 0 \\ B_x(\mathbf{k}) + iB_y(\mathbf{k}) & -B_z(\mathbf{k}) & \gamma \\ 0 & 0 & \mu(t) \end{pmatrix}, \tag{6}$$

where a term related to the identity matrix I_3 is neglected. Here, vector $\mathbf{B}(\mathbf{k})$ is obtained with the set of parameters $\{T_{ij}, A_{ij}, B_{ij}\}$. We note that the time-dependent $\mu(t)$ does not break the translational symmetry (or any other symmetry), allowing the exact diagonalization of H via that of each 3×3 matrix. Accordingly, the time evolution can also be computed via the complete set of 3×3 matrices.

Here, we focus on two points of particular interest: (i) We note that in k space, the central Hamiltonian can be expressed as

$$H_c = \sum_{\mathbf{k}} \begin{pmatrix} a_{\mathbf{k}}^\dagger & b_{\mathbf{k}}^\dagger \end{pmatrix} \mathbf{B}_{\mathbf{k}} \cdot \sigma \begin{pmatrix} a_{\mathbf{k}} \\ b_{\mathbf{k}} \end{pmatrix} \tag{7}$$

by Pauli matrices σ and then can be topologically nontrivial or not, depending on the explicit form of $\mathbf{B}_{\mathbf{k}}$. (ii) For a given $\mathbf{k}$, matrix $h_{\mathbf{k}}$ contains a Jordan block at instant $t = t_{\mathbf{k}}$, where $t_{\mathbf{k}}$ satisfies the equation

$$\mu(t_{\mathbf{k}}) = \pm|\mathbf{B}(\mathbf{k})|. \tag{8}$$

In this case, there are only two eigenstates for $h_{\mathbf{k}}$, which are the eigenstates of $\mathbf{B}_{\mathbf{k}} \cdot \sigma$, and then the completeness of eigenstates is spoiled.

Actually, in general, matrix $h_{\mathbf{k}}$ can be rewritten as

$$h_{\mathbf{k}} = |B(\mathbf{k})| \begin{pmatrix} \cos\theta_{\mathbf{k}} & \sin\theta_{\mathbf{k}} e^{-i\varphi_{\mathbf{k}}} & 0 \\ \sin\theta_{\mathbf{k}} e^{i\varphi_{\mathbf{k}}} & -\cos\theta_{\mathbf{k}} & \gamma_{\mathbf{k}} \\ 0 & 0 & \Delta_{\mathbf{k}} \end{pmatrix}, \tag{9}$$

where parameters in the matrix elements are defined as

$$\tan\theta_{\mathbf{k}} = \frac{B_z(\mathbf{k})}{|B(\mathbf{k})|}, \quad \tan\varphi_{\mathbf{k}} = \frac{B_y(\mathbf{k})}{B_x(\mathbf{k})},$$
$$\gamma_{\mathbf{k}} = \gamma/\varepsilon_{\mathbf{k}}, \quad \Delta_{\mathbf{k}} = \mu/\varepsilon_{\mathbf{k}}, \varepsilon_{\mathbf{k}} = |B(\mathbf{k})|. \tag{10}$$

Note that although matrix $h_{\mathbf{k}}$ is non-Hermitian, its eigenvalues are always real. Three eigenvectors are obtained as

$$|\psi_{\mathbf{k}}^{+}\rangle = \begin{pmatrix} \cos\frac{\theta_k}{2} \\ e^{i\varphi_k}\sin\frac{\theta_k}{2} \\ 0 \end{pmatrix}, \quad |\psi_{\mathbf{k}}^{-}\rangle = \begin{pmatrix} -\sin\frac{\theta_k}{2} \\ e^{i\varphi_k}\cos\frac{\theta_k}{2} \\ 0 \end{pmatrix},$$
$$|\psi_{\mathbf{k}}^{\Delta}\rangle = \frac{1}{\sqrt{\Lambda}}\begin{pmatrix} \gamma_k e^{-i\varphi_k}\sin\theta_k \\ \gamma_k(\Delta_k - \cos\theta_k) \\ \Delta_k^2 - 1 \end{pmatrix}, \tag{11}$$

with the eigenvalues

$$\varepsilon_{\mathbf{k}}^{\pm} = \pm\varepsilon_{\mathbf{k}}, \varepsilon_{\mathbf{k}}^{\Delta} = \Delta_k\varepsilon_{\mathbf{k}}, \tag{12}$$

where $\Lambda = \Delta_k^4 + \Delta_k^2\gamma_k^2 - 2\Delta_k^2 - 2\Delta_k\gamma_k^2\cos\theta_k + \gamma_k^2 + 1$ is the normalization coefficient in the context of a Dirac inner product. It shows that when taking $\Delta_{\mathbf{k}} = \pm 1$ or at $t = t_{\mathbf{k}}$, the matrix $h_{\mathbf{k}}$ reaches the EP. And we have $|\psi_{\mathbf{k}}^{\Delta}\rangle = |\psi_{\mathbf{k}}^{\pm}\rangle$; that is, the coalescing state appears, which is crucial for the scheme in this work.

III. EP DYNAMICS AND PERIODIC DRIVING

Based on the above analysis, the dynamics of H is governed by the time evolution operator

$$U(t) = \exp(-iHt) = \prod_{\mathbf{k}} U_{\mathbf{k}}(t), \tag{13}$$

where the time evolution operator in subspace $\mathbf{k}$ has the form

$$U_{\mathbf{k}}(t) = \mathcal{T}\exp[-i\int_0^t H_{\mathbf{k}}(t')dt'], \tag{14}$$

with $\mathcal{T}$ being the time-order operator. We first consider the case with slowly varying $H_{\mathbf{k}}(t)$ (i.e., very small ω). The time evolution around the instant $t = t_{\mathbf{k}}$ is crucial and can be described approximately by the operator

$$U_{\mathbf{k}}(t) \approx \exp[-iH_{\mathbf{k}}(t_{\mathbf{k}})t], \tag{15}$$

which obeys an exclusive EP dynamics.

We consider a time-independent $h_{\mathbf{k}}^{\mathrm{EP}}$ at the EP,

$$h_{\mathbf{k}}^{\mathrm{EP}} = \varepsilon_{\mathbf{k}}\begin{pmatrix} \cos\theta_{\mathbf{k}} & \sin\theta_{\mathbf{k}}e^{-i\varphi_{\mathbf{k}}} & 0 \\ \sin\theta_{\mathbf{k}}e^{i\varphi_{\mathbf{k}}} & -\cos\theta_{\mathbf{k}} & \gamma_{\mathbf{k}} \\ 0 & 0 & -1 \end{pmatrix}, \tag{16}$$

which contains a Jordan block, satisfying

$$h_{\mathbf{k}}^{\mathrm{EP}}|\psi_{\mathbf{k}}^{\pm}\rangle = \pm\varepsilon_{\mathbf{k}}|\psi_{\mathbf{k}}^{\pm}\rangle \tag{17}$$

and

$$A|\psi_{\mathbf{k}}^{\mathrm{a}}\rangle = |\psi_{\mathbf{k}}^{-}\rangle, \tag{18}$$

where the matrix

$$A = \left(\frac{h_{\mathbf{k}}^{\mathrm{EP}}}{\varepsilon_{\mathbf{k}}}\right)^2 - I_3 = \begin{pmatrix} 0 & 0 & -\sin\frac{\theta_k}{2} \\ 0 & 0 & e^{i\varphi_k}\cos\frac{\theta_k}{2} \\ 0 & 0 & 0 \end{pmatrix}. \tag{19}$$

Here, the vector

$$|\psi_{\mathbf{k}}^{\mathrm{a}}\rangle = (0, 0, 1)^{\mathrm{T}} \tag{20}$$

can be referred to as the auxiliary vector, while $|\psi_{\mathbf{k}}^{-}\rangle$ is the coalescing state of the matrix A since

$$A|\psi_{\mathbf{k}}^{-}\rangle = 0. \tag{21}$$

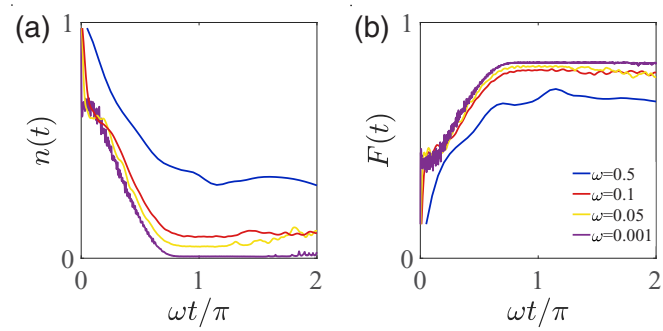

FIG. 2. Plots of $n(t)$ and $F(t)$, which are defined in Eqs. (29) and (30), obtained by exact diagonalization for the finite system. The parameters are $N = 20 \times 20$, $u = 1.2$, $\mu_0 = -2$, $W = 2.6$, and $\gamma = 0.5$. Four typical values of ω are taken and are indicated in the panels.

A straightforward derivation shows that

$$\exp\left(-ih_{\mathbf{k}}^{\mathrm{EP}}t\right) = -\frac{\gamma_k\varepsilon_{\mathbf{k}}t}{2}$$
$$\times[\sin(\varepsilon_{\mathbf{k}}t) + i(1 + 2\sin^2\frac{\varepsilon_{\mathbf{k}}t}{2})]A$$
$$+\cos(\varepsilon_{\mathbf{k}}t)I_3 - i\sin(\varepsilon_{\mathbf{k}}t)\left(\frac{h_{\mathbf{k}}^{\mathrm{EP}}}{\varepsilon_{\mathbf{k}}} + \frac{\gamma_k A}{2}\right). \tag{22}$$

The time evolution operator contains terms with linear and periodic functions of t. Then the time evolution for the initial state $|\psi_{\mathbf{k}}^{\mathrm{a}}\rangle$ is

$$|\psi_{\mathbf{k}}^{\mathrm{EP}}(t)\rangle = \exp\left(-ih_{\mathbf{k}}^{\mathrm{EP}}t\right)|\psi_{\mathbf{k}}^{\mathrm{a}}\rangle$$
$$= -\frac{\gamma_k\varepsilon_{\mathbf{k}}t}{2}\left[\sin(\varepsilon_{\mathbf{k}}t) + i\left(1 + 2\sin^2\frac{\varepsilon_{\mathbf{k}}t}{2}\right)\right]|\psi_{\mathbf{k}}^{-}\rangle$$
$$+\cos(\varepsilon_{\mathbf{k}}t)|\psi_{\mathbf{k}}^{\mathrm{a}}\rangle - i\sin(\varepsilon_{\mathbf{k}}t)\left(\frac{h_{\mathbf{k}}^{\mathrm{EP}}}{\varepsilon_{\mathbf{k}}}|\psi_{\mathbf{k}}^{\mathrm{a}}\rangle + \frac{\gamma_k}{2}|\psi_{\mathbf{k}}^{-}\rangle\right). \tag{23}$$

It indicates that the long-time evolution of the initial state $d_{\mathbf{k}}^{\dagger}|0\rangle_{\mathbf{k}}$ ($|0\rangle_{\mathbf{k}}$ is the vacuum state for operators $a_{\mathbf{k}}$, $b_{\mathbf{k}}$, and $d_{\mathbf{k}}$.) turns it into the coalescing state $|\psi_{\mathbf{k}}^{-}\rangle$ due to the linear-time dependence of the first term. Obviously, the action of $U_{\mathbf{k}}(t)$ at long times is the projection of any pure initial state on the component $|\psi_{\mathbf{k}}^{-}\rangle$, which is the perfect transport of the fermion from the source to the central system. For the many-particle case, we note that all the time-dependent $h_{\mathbf{k}}$ cannot reach their h_k^{EP} simultaneously. The dynamics for h_k near EP may result in the oscillation of the particle number between the source and the central systems, although the hopping term is unidirectional. Nevertheless, periodically varying $\mu(t)$ passing by the EP of every $h_{\mathbf{k}}$ is expected to transport the fermion from the source to the central system in each $\mathbf{k}$ sector almost completely. Ideally, if this occurs in every $\mathbf{k}$ sector, the fully filled initial state

$$\prod_j d_j^{\dagger}|0\rangle = \prod_{\mathbf{k}} d_{\mathbf{k}}^{\dagger}|0\rangle \tag{24}$$

will evolve to the ground state of the central system, while becoming empty in the source system. Note that the initial state is a trivial many-particle state, a saturated filled state.

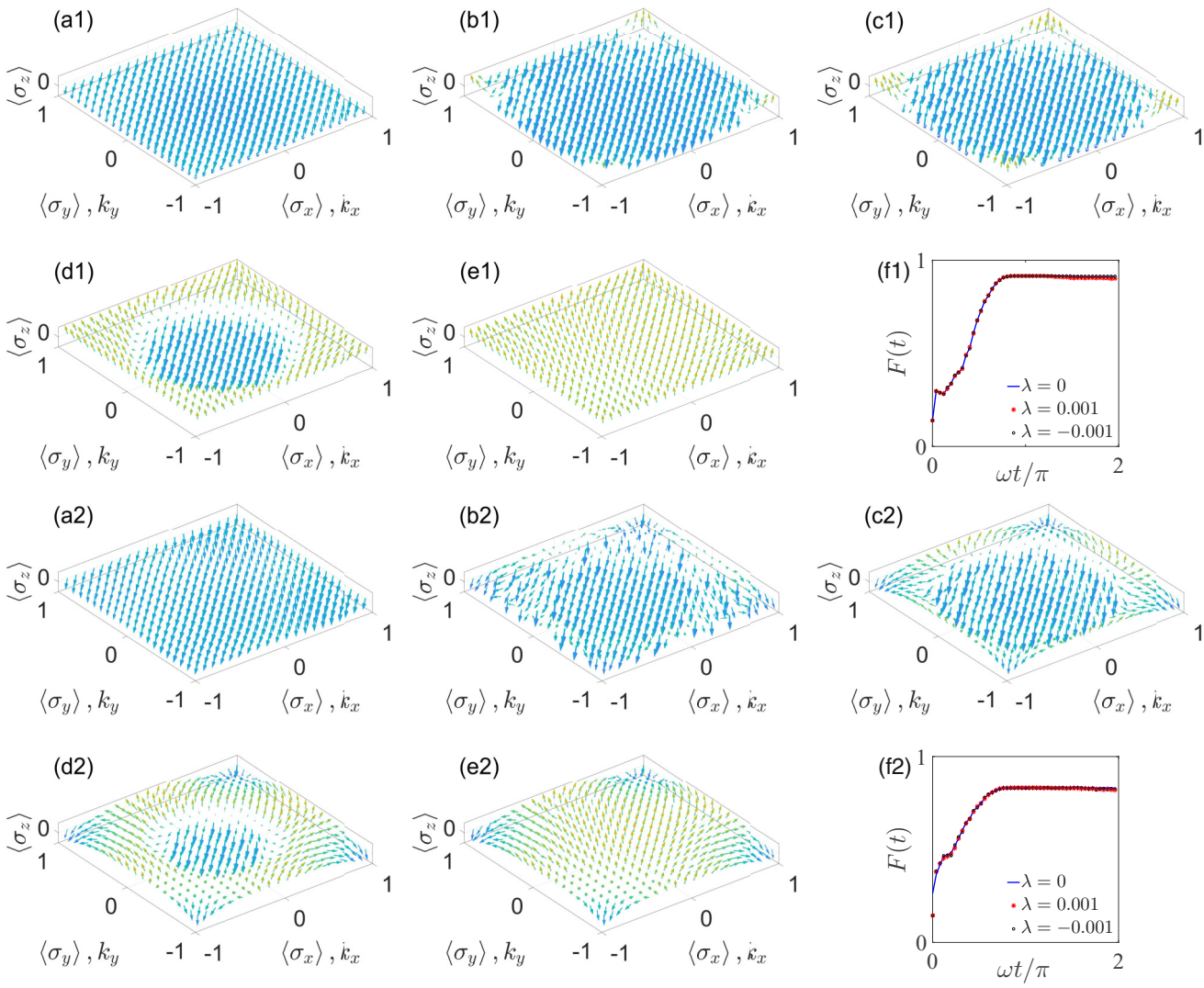

FIG. 3. Plots of the skyrmion pattern at several typical instants, which are defined in Eq. (32), obtained by exact diagonalization of the finite system. The corresponding fidelity is also plotted for comparison. The parameters are $N = 20 \times 20$, $\omega = 0.001$, $\gamma = 0.5$, and (a1)–(d1) $u = 3.2$, $\mu_0 = -3.21$, $W = 3.94$ and (a2)–(d2) $u = 1.2$, $\mu_0 = -2$, $W = 2.38$, which correspond to the central systems in topologically trivial and nontrivial phases, respectively. (f1) and (f2) are the plots of fidelity, which is defined in Eq. (30). Three typical values of λ are taken and indicated in the panels.

The aim of the scheme is to prepare a nontrivial state from such an initial state through the time evolution in the context of non-Hermitian quantum mechanics.

To illustrate our scheme and investigate its efficiency, we consider the central system as a QWZ model introduced by Qi *et al.* [26]. The Bloch Hamiltonian is

$$h_{\mathbf{k}} = B_x\sigma_x + B_y\sigma_y + B_z\sigma_z, \tag{25}$$

where the field components are

$$\begin{aligned} &B_x = \sin k_x, B_y = \sin k_y, \\ &B_z = u + \cos k_x + \cos k_y. \end{aligned} \tag{26}$$

It is well known that the Chern number of the lower band is

$$\begin{aligned} &c = 0, \quad |u| > 2, \\ &c = \pm 1, \quad 0 < \pm u < 2. \end{aligned} \tag{27}$$

Numerical simulation is performed to verify the efficiency of the scheme. Here, the computation of the time-ordered integral is performed using a uniform mesh in the time discretization for the time-dependent Hamiltonian $h_{\mathbf{k}}(t)$ with different ω. We compute the time evolution for the initial state $|\psi_{\mathbf{k}}(0)\rangle = d_{\mathbf{k}}^{\dagger}|0\rangle_{\mathbf{k}}$ and compare the evolved state $|\psi_{\mathbf{k}}(t)\rangle$ with the target state

$$|\psi_{\mathbf{k}}^{c}\rangle = \left(\sin\frac{\theta_k}{2}a_{\mathbf{k}}^{\dagger} - e^{i\varphi_k}\cos\frac{\theta_k}{2}b_{\mathbf{k}}^{\dagger}\right)|0\rangle_{\mathbf{k}}, \tag{28}$$

which is the coalescing state of $h_{\mathbf{k}}$ [Eq. (25)] at the EP with negative energy. The observables are the particle number left in the source system

$$n(t) = \frac{1}{N}\sum_{\mathbf{k}}\frac{\langle\psi_{\mathbf{k}}(t)|d_{\mathbf{k}}^{\dagger}d_{\mathbf{k}}|\psi_{\mathbf{k}}(t)\rangle}{||\psi_{\mathbf{k}}(t)\rangle|^2} \tag{29}$$

and the fidelity

$$F(t)=\frac{1}{N}\sum_{\mathbf{k}}\frac{\left|\langle\psi_{\mathbf{k}}^{c}|\psi_{\mathbf{k}}(t)\rangle\right|}{\left|\left|\psi_{\mathbf{k}}^{c}\rangle|\psi_{\mathbf{k}}(t)\rangle\right|\right|}, \tag{30}$$

which measure the efficiency of the transport. The numerical results for finite systems with presentative parameters are plotted in Fig. 2. We see that the optimal efficiency occurs when $\omega=0.001$, and the transport efficiency decreases gradually with the increasing of ω.

We also compute the time-dependent skyrmion to characterize the formation process of the target state. To this end we introduce the auxiliary matrices

$$\Sigma_{\alpha}=\begin{pmatrix}\sigma_{\alpha} & 0\\ 0 & 1\end{pmatrix},\quad \Sigma_{0}=\begin{pmatrix}I_{2} & 0\\ 0 & 1\end{pmatrix}, \tag{31}$$

where σ_{α} is Pauli matrix in the α ($\alpha=x,y,z$) component and I_2 is the unit matrix. The time-dependent skyrmion is evaluated as

$$\langle\sigma_{\alpha}\rangle_{\mathbf{k},t}=\frac{\langle\psi_{\mathbf{k}}(t)|\Sigma_{\alpha}|\psi_{\mathbf{k}}(t)\rangle}{\langle\psi_{\mathbf{k}}(t)|\Sigma_{0}|\psi_{\mathbf{k}}(t)\rangle}. \tag{32}$$

Unlike the expectation value of the Pauli matrix σ_{α} in the usual study [27], $\langle\sigma_{\alpha}\rangle_{\mathbf{k},0}=0$ for all α and $\sum_{\alpha=x,y,z}(\langle\sigma_{\alpha}\rangle_{\mathbf{k},t})^{2}\leqslant 1$. In the case in which all the fermions have been transported to the central system in the long-time limit the skyrmion obeys the pattern

$$\langle\sigma\rangle_{\mathbf{k},\infty}=\frac{\mathbf{B}(\mathbf{k})}{|\mathbf{B}(\mathbf{k})|}, \tag{33}$$

which characterizes the topological feature of the phase. The numerical results for finite systems with presentative parameters $\langle\sigma_{\alpha}\rangle_{\mathbf{k},t}$ at different times are plotted in Fig. 3. Figures 3(e1) and 3(e2) clearly show that in the long-time limit the skyrmion exhibits approximately the pattern defined in Eq. (33), corresponding to the central systems in topologically trivial and nontrivial phases, respectively. In Figs. 3(f1) and 3(f2), we recalculate the fidelity by adding a back-hopping term, i.e., $H_{\text{in}}\rightarrow H_{\text{in}}=\gamma\sum_{j=1}^{N}b_{j}^{\dagger}d_{j}+\lambda\gamma\sum_{j=1}^{N}d_{j}^{\dagger}b_{j}$, where a small λ controls the situation near the EP ($\lambda>0$) and symmetry breaking ($\lambda<0$), respectively. The results show that the small back-hopping term does not influence the efficiency of the scheme too much. In the Appendix, we present a detailed derivation.

IV. EDGE STATE ENGINEERING

The aforementioned formalism is developed in the system with translational symmetry in order to simplify the calculation procedure. This section will be devoted to the realization of quantum mold casting in a system without the translational symmetry. The essential step for this extension is replacing the index $\mathbf{k}$ by the eigenmodes of H_{c}. The fact that the flat band of H_{s} and uniform hopping in H_{in}, still allow H to be block diagonalizable.

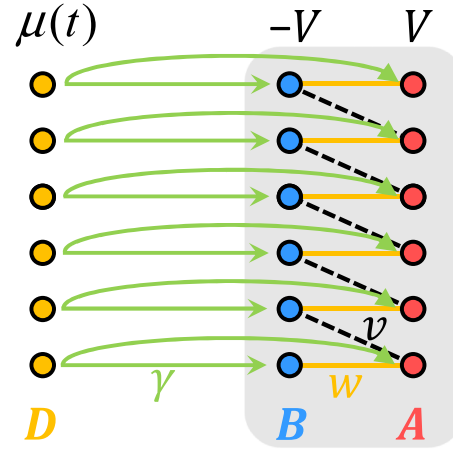

FIG. 4. Schematic of the system with a generalized RM chain as the central system H_{c}. Each part of the system is represented by Eqs. (34) and (35).

To demonstrate this point, we consider the central system H_{c} to be a generalized RM chain with the Hamiltonian

$$H_{\text{c}}=\sum_{j=1}^{N-1}\left(w_{j}a_{j}^{\dagger}b_{j}+v_{j}a_{j+1}^{\dagger}b_{j}+\text{H.c.}\right)+V\sum_{j=1}^{N}\left(a_{j}^{\dagger}a_{j}-b_{j}^{\dagger}b_{j}\right), \tag{34}$$

where w_j and v_j are position-dependent hopping amplitudes (including random distributions). The other Hamiltonians have a slight change from their original forms,

$$H_{\text{s}}=\mu(t)\sum_{j=1}^{N}d_{j}^{\dagger}d_{j},\quad H_{\text{in}}=\gamma\sum_{j=1}^{N}\left(a_{j}^{\dagger}d_{j}+b_{j}^{\dagger}d_{j}\right). \tag{35}$$

A schematic of the system is presented in Fig. 4. The Hamiltonian H_{c} can be written as the diagonal-block form

$$H=\sum_{n=1}^{N}H_{n}, \tag{36}$$

$$H_{n}=\begin{pmatrix}f_{a,n}^{\dagger} & f_{b,n}^{\dagger} & f_{d,n}^{\dagger}\end{pmatrix}h_{n}\begin{pmatrix}f_{a,n}\\ f_{b,n}\\ f_{d,n}\end{pmatrix}, \tag{37}$$

which reduces the eigenproblem of the present H to that of the 3×3 matrix. Here, the Bloch-like matrix h_n has the form

$$h_{n}=\begin{pmatrix}V & \varepsilon_{0}(n) & \gamma\\ \varepsilon_{0}(n) & -V & \gamma\\ 0 & 0 & \mu(t)\end{pmatrix}, \tag{38}$$

and three sets of canonical fermion operators are defined as

$$f_{a,n}^{\dagger}=\sum_{j=1}^{N}A_{j}^{n}a_{j}^{\dagger},\ f_{b,n}^{\dagger}=\sum_{j=1}^{N}B_{j}^{n}b_{j}^{\dagger},\quad f_{d,n}^{\dagger}=\sum_{j=1}^{N}B_{j}^{n}d_{j}^{\dagger}, \tag{39}$$

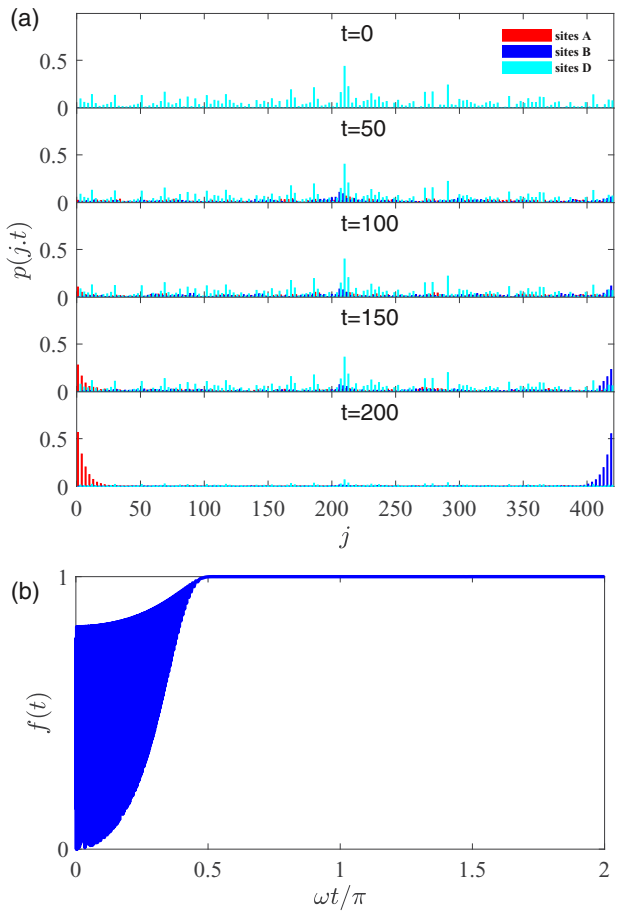

FIG. 5. (a) The profiles of $p(j,t)$ at several typical instants, defined in Eq. (49), showing the formation of the edge state. (b) Corresponding fidelity defined in Eq. (52). The parameters are $N = 140, V = 0, v = 5, w = 3, \mu_0 = 0, W = 2, \gamma = 0.5, \omega = 0.001$.

with real coefficients A_j^n and B_j^n being obtained by single-particle eigenstates of H_c at $V = 0$, with eigenvalues $\pm\varepsilon_0(n)$, satisfying the orthonormal complete relations

$$\sum_j \left(A_j^m\right)^* A_j^n = \sum_j \left(B_j^m\right)^* B_j^n = \delta_{mn},$$
$$\sum_n (A_i^n)^* A_j^n = \sum_n (B_i^n)^* B_j^n = \delta_{ij}. \tag{40}$$

Actually, the Hamiltonian of the SSH chain is diagonalized as

$$H_c(V=0) = \sum_{n=1}^{N} \varepsilon_0(n)(f_{+,n}^\dagger f_{+,n} - f_{-,n}^\dagger f_{-,n}), \tag{41}$$

where $\varepsilon_0(n) > 0$ is the positive energy spectrum with $n \in [1, N]$ and

$$f_{\pm,n}^\dagger = \frac{1}{\sqrt{2}}(f_{a,n}^\dagger \pm f_{b,n}^\dagger) \tag{42}$$

due to the fact that the SSH chain is a bipartite lattice. We note that h_n is essentially the counterpart of $h_{\mathbf{k}}$ in Eq. (9) with a slight difference. The time evolution driven by h_n is similar to that of $h_{\mathbf{k}}$, including the EP dynamics.

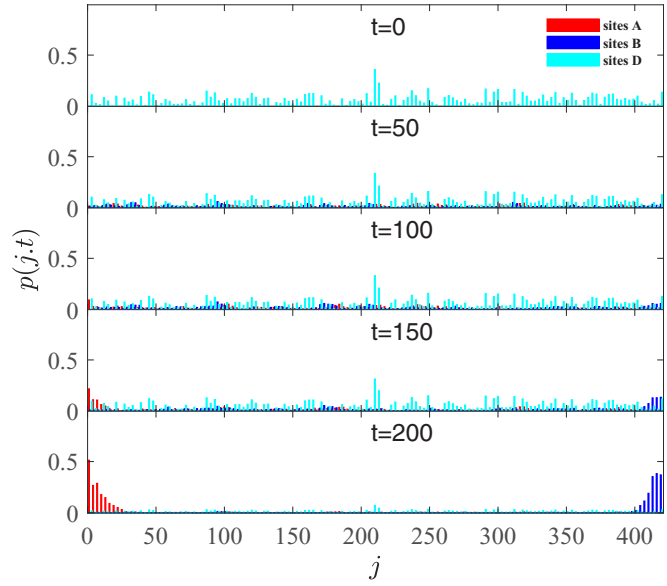

FIG. 6. The profiles of $p(j,t)$ at several typical instants in the presence of random perturbations with different random strengths w_j and v_j defined in Eq. (51). The parameters are $N = 140, V = 0, v = 5, w = 3, \mu_0 = 0, W = 2, \gamma = 0.5, \omega = 0.001, R = 1.2$.

The central system H_c is the simplest prototype of a topologically nontrivial band insulator with a symmetry-protected topological phase [28,29]. In recent years, it has attracted much attention, and extensive studies have been carried out [30–37]. In the uniform case, $w = w_j < v = v_j$, there are two edge sates with eigenvalues $\pm V$ for large N, which are explicitly expressed as

$$|\mathrm{L}\rangle = \Omega \sum_{j=1}^{N} \left(-\frac{w}{v}\right)^{j-1} a_j^\dagger |0\rangle, \tag{43}$$

$$|\mathrm{R}\rangle = \Omega \sum_{j=1}^{N} \left(-\frac{w}{v}\right)^{N-j} b_j^\dagger |0\rangle, \tag{44}$$

where the normalization factor is $\Omega = \sqrt{1 - (\frac{w}{v})^2}$. In addition, small random perturbations on w and v cannot remove the edge states or change their eigenvalues. Taking a suitable value of V, two edge states can lie within the gap of the spectrum. In the following, we perform a numerical simulation of the time evolution for the fully filled initial state

$$|\psi(0)\rangle = \prod_j d_j^\dagger |0\rangle = \prod_n d_n^\dagger |0\rangle \tag{45}$$

by taking several different values of ω in $\mu(t)$. The evolved state obeys

$$|\psi(t)\rangle = \prod_n |\psi_n(t)\rangle = U(t) \prod_n d_n^\dagger |0\rangle, \tag{46}$$

where the time evolution operator has a form similar to Eq. (13),

$$U(t) = \prod_n U_n(t), \tag{47}$$

and the time evolution operator in subspace n has the form

$$U_n(t) = \mathcal{T} \exp[-i \int_0^t H_n(t')dt']. \tag{48}$$

The purpose of this process is the generation of a single-particle edge state in H_c at levels $V = 0$, which is isolated in the midgap.

We define the time-dependent distribution of particle probability $p(j,t)$ in the central system as

$$\begin{aligned} p(3l-2,t) &= |\langle 0|a_l|\psi(t)\rangle|, \\ p(3l-1,t) &= |\langle 0|b_l|\psi(t)\rangle|, \\ p(3l,t) &= |\langle 0|d_l|\psi(t)\rangle| \end{aligned} \tag{49}$$

for the evolved state to measure the efficiency of the scheme. Ideally, the target state with a perfect edge state has the distribution $p_{\mathrm{E}}(j)$,

$$\begin{aligned} p_{\mathrm{E}}(3l-2) &= \Omega^2\left(\frac{w}{v}\right)^{4l-2}, \\ p_{\mathrm{E}}(3l-1) &= \Omega^2\left(\frac{w}{v}\right)^{2N-2l}, \\ p_{\mathrm{E}}(3l) &= 0. \end{aligned} \tag{50}$$

In the case with nonuniform distributions $\{w_j\}$ and $\{v_j\}$, the corresponding p_{E} can be obtained numerically from exact diagonalization of the Hamiltonian.

Numerical simulations of the formation processes of the single-particle edge state in the absence and presence of random perturbations with different random strengths. The computation is performed by taking two sets of random numbers, $\{w_j\}$ and $\{v_j\}$, around w and v, i.e.,

$$w_j = w + \mathrm{ran}(-R,R),\ v_j = v + \mathrm{ran}(-R,R), \tag{51}$$

where $\mathrm{ran}(-R,R)$ denotes a uniform random number within $(-R,R)$. We employ the fidelity

$$f(t) = |\langle \psi_{\mathrm{T}}|\psi(t)\rangle| \tag{52}$$

to characterize the efficiency of the scheme, where the target state $|\psi_{\mathrm{T}}\rangle$ is the midgap state. The profiles of $p(j,t)$ for several representative situations with fixed w and v are presented in Fig. 5, and profiles with different random strengths $\{w_j\}$ and $\{v_j\}$ are presented in Fig. 6. We can see that the evolved state with fixed w and v is very close to the perfect edge state. In the presence of random perturbations, although the probability distribution seems to be irregular, it is evidently the edge state. These results agree with our predictions. This scheme can be extended to the cases with nonzero V or two- and three-dimensional central systems for preparing edge and surface states. Unlike the bulk states, these states are responsible for the topological features. Furthermore, we consider the nonzero V term to show that the scheme has a wide range of applications. (i) For $V = 0$, which we discussed above, the two energy levels corresponding to the two edge states degenerate at zero. Due to the degeneracy of the states, we can get an edge state where one half is on the left and the other half is on the right, as shown in Figs. 5 and 6. (ii) For $V \neq 0$, the degenerate midgap zero-energy levels are separated by a magnitude of $2V$. Two edge states are still robust under the random perturbations on the hopping terms, but we can get only either a left edge state (red one) or a right edge state (blue one) at a time. Numerical simulations for nonzero V are the same as those in Figs. 5 and 6, but a set of parameters has only the half of the plots.

V. SUMMARY

In summary, we presented a scheme to realize quantum mold casting, i.e., engineering a target quantum state on demand by the time evolution of a trivial initial state. The underlying mechanism is EP dynamics. We have proposed a quantum mold model for dynamically casting stable topological insulating states and edge states. We introduced the periodic driving chemical potential, which causes EPs to exist in different subspaces and allows fermions to be transferred from the fully filled trivial source system to the corresponding subspaces of the topological central system. As examples, we considered the central system to be the QWZ model and a generalized RM model to dynamically cast topological insulating states and edge states, respectively. Numerical simulations showed that the scheme is efficient. The advantage of the scheme is that the robust topological edge and surface states can be engineered without filling the whole valence band.

ACKNOWLEDGMENT

We acknowledge the support of the NSFC (Grant No. 11874225).

APPENDIX

Here, we provide a way to understand what happens to the efficiency of the scheme if the system deviates slightly from the EP. We start by considering a two-level system with

$$h = \begin{pmatrix} 0 & 1 \\ \lambda & 0 \end{pmatrix}. \tag{A1}$$

It has time-reversal symmetry, i.e., $\mathcal{T}h\mathcal{T}^{-1}=h$, where $\mathcal{T}\sqrt{-1}\mathcal{T}^{-1}=-\sqrt{-1}$ is the conjugation operator. The eigenvectors and eigenvalues are expressed as

$$|\phi_\pm\rangle = \frac{1}{\sqrt{|\lambda|+1}}\begin{pmatrix} \pm 1 \\ \sqrt{\lambda} \end{pmatrix}, \tag{A2}$$

$$\varepsilon_\pm = \pm\sqrt{\lambda}, \tag{A3}$$

which indicates that the EP occurs at $\lambda = 0$. For a given initial state

$$|\psi(0)\rangle = \frac{1}{\sqrt{|a|^2+|b|^2}}\begin{pmatrix} a \\ b \end{pmatrix}, \tag{A4}$$

the time-evolved state $|\psi(t)\rangle$ can be obtained for following three cases.

(i) For $\lambda = 0$, the system is at the EP. The time evolution operator is

$$U(t) = e^{-iht} = 1 - it\begin{pmatrix} 0 & 1 \\ 0 & 0 \end{pmatrix} \tag{A5}$$

because $\left(\begin{smallmatrix} 0 & 1 \\ 0 & 0 \end{smallmatrix}\right)^2 = 0$. Then we have

$$|\psi(t)\rangle = \frac{1}{\sqrt{|a|^2+|b|^2}}\left[\begin{pmatrix} a \\ b \end{pmatrix} - it\begin{pmatrix} b \\ 0 \end{pmatrix}\right]. \tag{A6}$$

(ii) For $\lambda > 0$, the eigenvalues are real since the symmetry is not broken, $\mathcal{T}|\phi_\pm\rangle = |\phi_\pm\rangle$. For nonzero λ, we always have

$$|\psi(0)\rangle = \frac{1}{\sqrt{|a|^2+|b|^2}}\begin{pmatrix} a \\ b \end{pmatrix} = \frac{\sqrt{|\lambda|+1}}{2\sqrt{|a|^2+|b|^2}}\left(\frac{b}{\sqrt{\lambda}}+a\right)|\phi_+\rangle + \left(\frac{b}{\sqrt{\lambda}}-a\right)|\phi_-\rangle. \tag{A7}$$

Then we have

$$|\psi(t)\rangle = \frac{\sqrt{|\lambda|+1}}{2\sqrt{|a|^2+|b|^2}}\left[\left(\frac{b}{\sqrt{\lambda}}+a\right)e^{-i\sqrt{\lambda}t}|\phi_+\rangle + \left(\frac{b}{\sqrt{\lambda}}-a\right)e^{i\sqrt{\lambda}t}|\phi_-\rangle\right], \tag{A8}$$

which is a periodic function with period $2\pi/\sqrt{\lambda}$. For small $\sqrt{\lambda}t$, we have

$$|\psi(t)\rangle \approx \frac{\sqrt{|\lambda|+1}}{\sqrt{|a|^2+|b|^2}}\left[\begin{pmatrix} a \\ b \end{pmatrix} - it\begin{pmatrix} b \\ 0 \end{pmatrix} - ia\lambda t\begin{pmatrix} 0 \\ 1 \end{pmatrix}\right]. \tag{A9}$$

(iii) For $\lambda < 0$, the eigenvalues are imaginary, and the time-reversal symmetry is broken, i.e., $\mathcal{T}|\phi_+\rangle = |\phi_-\rangle \neq c|\phi_+\rangle$. In this case, we have

$$|\psi(t)\rangle = \frac{\sqrt{|\lambda|+1}}{2\sqrt{|a|^2+|b|^2}}\left[\left(\frac{b}{\sqrt{\lambda}}+a\right)e^{\sqrt{|\lambda|}t}|\phi_+\rangle + \left(\frac{b}{\sqrt{\lambda}}-a\right)e^{-\sqrt{|\lambda|}t}|\phi_-\rangle\right], \tag{A10}$$

which is not a periodic function. However, for small $\sqrt{|\lambda|}t$, we still have

$$|\psi(t)\rangle \approx \frac{\sqrt{|\lambda|+1}}{\sqrt{|a|^2+|b|^2}}\left[\begin{pmatrix} a \\ b \end{pmatrix} - it\begin{pmatrix} b \\ 0 \end{pmatrix} - ia\lambda t\begin{pmatrix} 0 \\ 1 \end{pmatrix}\right]. \tag{A11}$$

In summary, the dynamics of systems with small but nonzero λ are the same as those of zero λ, within the duration $\sqrt{|\lambda|}t \ll 1$, i.e.,

$$|\psi(t)\rangle \approx \frac{1}{\sqrt{|a|^2+|b|^2}}\left[\begin{pmatrix} a \\ b \end{pmatrix} - it\begin{pmatrix} b \\ 0 \end{pmatrix}\right]. \tag{A12}$$

This result indicates that the EP dynamics can be extended to the near-EP dynamics. The efficiency of the scheme does not change suddenly when the system deviates slightly from the EP.

[1] T. Oka and H. Aoki, Photovoltaic Hall effect in graphene, Phys. Rev. B **79**, 081406(R) (2009).

[2] T. Kitagawa, T. Oka, A. Brataas, L. Fu, and E. Demler, Transport properties of nonequilibrium systems under the application of light: Photoinduced quantum Hall insulators without Landau levels, Phys. Rev. B **84**, 235108 (2011).

[3] M. S. Rudner, N. H. Lindner, E. Berg, and M. Levin, Anomalous Edge States and the Bulk-Edge Correspondence for Periodically Driven Two-Dimensional Systems, Phys. Rev. X **3**, 031005 (2013).

[4] L. E. F. Foa Torres, P. M. Perez-Piskunow, C. A. Balseiro, and G. Usaj, Multiterminal Conductance of a Floquet Topological Insulator, Phys. Rev. Lett. **113**, 266801 (2014).

[5] H. Dehghani, T. Oka, and A. Mitra, Out-of-equilibrium electrons and the Hall conductance of a Floquet topological insulator, Phys. Rev. B **91**, 155422 (2015).

[6] J. H. Wilson, J. C. W. Song, and G. Refael, Remnant Geometric Hall Response in a Quantum Quench, Phys. Rev. Lett. **117**, 235302 (2016).

[7] N. H. Lindner, G. Refael, and V. Galitski, Floquet topological insulator in semiconductor quantum wells, Nat. Phys. **7**, 490 (2011).

[8] J. Cayssol, B. Dora, F. Simon, and R. Moessner, Floquet topological insulators, Phys. Status Solidi RRL **7**, 101 (2013).

[9] M. Thakurathi, A. A. Patel, D. Sen, and A. Dutta, Floquet generation of Majorana end modes and topological invariants, Phys. Rev. B **88**, 155133 (2013).

[10] A. Kundu and B. Seradjeh, Transport Signatures of Floquet Majorana Fermions in Driven Topological Superconductors, Phys. Rev. Lett. **111**, 136402 (2013).

[11] C. M. Bender and S. Boettcher, Real Spectra in Non-Hermitian Hamiltonians Having PT Symmetry, Phys. Rev. Lett. **80**, 5243 (1998).

[12] C. M. Bender, D. C. Brody, and H. F. Jones, Complex Extension of Quantum Mechanics, Phys. Rev. Lett. **89**, 270401 (2002).

[13] A. Mostafazadeh, Pseudo-Hermiticity versus PT symmetry: The necessary condition for the reality of the spectrum of a non-Hermitian Hamiltonian, J. Math. Phys. **43**, 205 (2002); Pseudo-Hermiticity versus PT-symmetry. II. A complete characterization of non-Hermitian Hamiltonians with a real spectrum, **43**, 2814 (2002); Pseudo-Hermiticity versus PT-symmetry III: Equivalence of pseudo-Hermiticity and the presence of antilinear symmetries, **43**, 3944 (2002); Pseudo-supersymmetric quantum mechanics and isospectral pseudo-Hermitian Hamiltonians, Nucl. Phys. B **640**, 419 (2002); Pseudo-Hermiticity and generalized PT- and CPT-symmetries, J. Math. Phys. **44**, 974 (2003).

[14] W. D. Heiss, The physics of exceptional points, J. Phys. A **45**, 444016 (2012).

[15] I. Rotter, A non-Hermitian Hamilton operator and the physics of open quantum systems, J. Phys. A **42**, 153001 (2009); I. Rotter and A. F. Sadreev, Avoided level crossings, diabolic points, and branch points in the complex plane in an open double quantum dot, Phys. Rev. E **71**, 036227 (2005).

[16] H. Xu, D. Mason, L. Jiang, and J. G. E. Harris, Topological energy transfer in an optomechanical system with exceptional points, Nature (London) **537**, 80 (2016).

[17] B. F. Samsonov, Spectral singularities of non-Hermitian Hamiltonians and SUSY transformations, J. Phys. A **38**, L571 (2005).

[18] A. A. Andrianov, F. Cannata, and A. V. Sokolov, Spectral singularities for non-Hermitian one-dimensional Hamiltonians: Puzzles with resolution of identity, J. Math. Phys. **51**, 052104 (2010).

[19] A. Mostafazadeh, Spectral Singularities of Complex Scattering Potentials and Infinite Reflection and Transmission Coefficients

at Real Energies, Phys. Rev. Lett. **102**, 220402 (2009); Optical spectral singularities as threshold resonances, Phys. Rev. A **83**, 045801 (2011).

[20] S. Longhi, Spectral singularities in a non-Hermitian Friedrichs-Fano-Anderson model, Phys. Rev. B **80**, 165125 (2009); Spectral singularities and Bragg scattering in complex crystals, Phys. Rev. A **81**, 022102 (2010).

[21] X. Z. Zhang, L. Jin, and Z. Song, Perfect state transfer in $\mathcal{PT}$-symmetric non-Hermitian networks, Phys. Rev. A **85**, 012106 (2012).

[22] X. Z. Zhang, L. Jin, and Z. Song, Dynamic magnetization in non-Hermitian quantum spin systems, Phys. Rev. B **101**, 224301 (2020).

[23] X. Z. Zhang and Z. Song, Dynamical preparation of a steady ODLRO state in the Hubbard model with local non-Hermitian impurity, Phys. Rev. B **102**, 174303 (2020).

[24] X. M. Yang and Z. Song, Resonant generation of a *p*-wave Cooper pair in a non-Hermitian Kitaev chain at the exceptional point, Phys. Rev. A **102**, 022219 (2020).

[25] H. Weng, R. Yu, X. Hu, X. Dai, and Z. Fang, Quantum anomalous Hall effect and related topological electronic states, Adv. Phys. **64**, 227 (2015).

[26] X.-L. Qi, Y.-S. Wu, and S.-C. Zhang, Topological quantization of the spin Hall effect in two-dimensional paramagnetic semiconductors, Phys. Rev. B **74**, 085308 (2006).

[27] S. Lin and Z. Song, Wide-range-tunable Dirac-cone band structure in a chiral-time-symmetric non-Hermitian system, Phys. Rev. A **96**, 052121 (2017).

[28] S. Ryu and Y. Hatsugai, Topological Origin of Zero-Energy Edge States in Particle-Hole Symmetric Systems, Phys. Rev. Lett. **89**, 077002 (2002).

[29] X.-G. Wen, Symmetry-protected topological phases in noninteracting fermion systems, Phys. Rev. B **85**, 085103 (2012).

[30] D. Xiao, M. C. Chang, and Q. Niu, Berry phase effects on electronic properties, Rev. Mod. Phys. **82**, 1959 (2010).

[31] M. Z. Hasan and C. L. Kane, Colloquium: Topological insulators, Rev. Mod. Phys. **82**, 3045 (2010); X.-L. Qi and S.-C. Zhang, Topological insulators and superconductors, *ibid.* **83**, 1057 (2011).

[32] P. Delplace, D. Ullmo, and G. Montambaux, Zak phase and the existence of edge states in graphene, Phys. Rev. B **84**, 195452 (2011).

[33] L. Li, Z. Xu, and S. Chen, Topological phases of generalized Su-Schrieffer-Heeger models, Phys. Rev. B **89**, 085111 (2014).

[34] L. Li and S. Chen, Characterization of topological phase transitions via topological properties of transition points, Phys. Rev. B **92**, 085118 (2015).

[35] S. Lin, X. Z. Zhang, C. Li, and Z. Song, Long-range entangled zero-mode state in a non-Hermitian lattice, Phys. Rev. A **94**, 042133 (2016).

[36] R. Wang and Z. Song, Dynamical topological invariant for the non-Hermitian Rice-Mele model, Phys. Rev. A **98**, 042120 (2018).

[37] R. Wang and Z. Song, Robustness of the pumping charge to dynamic disorder, Phys. Rev. B **100**, 184304 (2019).